19th Brazilian Congress of Thermal Sciences and Engineering
November 06th-10th, 2022, Bento Gonçalves - RS - Brazil

ENC-2022-0325
EXPERIMENTAL ANALYSIS OF THE HEAT AND MASS TRANSFER OF A FLAT SHEET MODULE OF DIRECT CONTACT MEMBRANE DISTILLATION (DCMD) FOR DESALINATION

Cristiane Raquel Sousa Mesquita
Ingrid Vasconcelos Curcino
Abdul Orlando Cárdenas Gómez
Laboratory of Nano & Microfluidics and Microsystems - LabMEMS, Mechanical Eng. Dept., POLI & COPPE/UFRJ, Universidade Federal do Rio de Janeiro, Rio de Janeiro/RJ, Brazil
crismesquita@coppe.ufrj.br, ingrid.curcino@mecanica.coppe.ufrj.br, orlandocardenas1589@gmail.com

Joao Alves de Lima [a,b]
[a] Laboratory of Nano & Microfluidics and Microsystems - LabMEMS, Mechanical Eng. Dept., POLI & COPPE/UFRJ, Universidade Federal do Rio de Janeiro, Rio de Janeiro/RJ, Brazil
[b] Renewable Energy Eng. Dept., DEER/CEAR/UFPB, Federal University of Paraíba, João Pessoa, PB, Brazil
jalima@cear.ufpb.br

Carolina Palma Naveira-Cotta [a]
Renato Machado Cotta [a,c]
[a] Laboratory of Nano & Microfluidics and Microsystems - LabMEMS, Mechanical Eng. Dept., POLI & COPPE/UFRJ, Universidade Federal do Rio de Janeiro, Rio de Janeiro/RJ, Brazil
[c] General Directorate of Nuclear and Technological Development, DGGDNTM, Brazilian Navy, Rio de Janeiro, RJ, Brazil.
carolina@mecanica.coppe.ufrj.br, cotta@mecanica.coppe.ufrj.br

Abstract. *The growing interest in membrane distillation (MD) as a promising and competing technology in desalination is mainly due to (i) the ability to provide rejection of non-volatile feed solutes very close to 100%, and; (ii) operation at ambient pressure and temperatures, favoring the use of low exergy heat sources, heat from solar collectors and photovoltaic panels of high concentration. Experimental benches allow the characterization of a single membrane in a controlled environment through the reproduction of operational temperature conditions (60-90 °C). Among all MD configurations, the DCMD (Direct Contact Membrane Distillation) is the most suitable for laboratory-scale studies; its simplicity of installation and operation and small number of process parameters make it more suitable for the characterization and evaluation performance of different types of membranes. In this context, the study presents a theoretical-experimental analysis of the heat and mass transfer process in a DCMD module. The experiments were carried out in a flat sheet module under operating conditions reproduced according to the 2k factorial experimental design, with different levels of NaCl concentration in the feed solution, where the distillate mass flux obtained experimentally were compared with the results obtained through a theoretical model for distillate flux prediction. Overall, the theoretical and experimental results showed good agreement with each other, and with similar works with the DCMD configuration, such as a decrease in the permeate flux with the increase of the salinity in the feed solution, although they indicate that there is a slight underestimation by the theoretical lumped model, which can be attributed to the simplifications in the model's design and inaccuracies of the input data of the membrane (thickness, contact angle, porosity and pore size distribution).*

Keywords: *Desalination, Direct contact membrane distillation, Heat and mass transfer, hydrophobic membrane.*

1. INTRODUCTION

Population growth and climate change have led to an increase in the consumption of drinking water and energy, so this growing water demand has become one of the most crucial challenges in most countries around the world (Huo et al. 2021; X. Li et al. 2021; Z. Li, Wang, and Che 2021; Wu et al. 2021).Thus, designing efficient wastewater treatment systems has attracted much attention in developing countries (Emeh and Igwe 2018; Fan et al. 2021; Moondra, 2021).

Essential factors in desalination market research are focused on reducing energy consumption, system costs, and pollutant emissions. Thermal and membrane separation processes are known as the most used desalination methods. Membrane distillation (MD) is a thermally driven separation technique that relies on the transport of vapor through a microporous membrane, displayed as a barrier to the liquid phase, where the pores of the membrane will allow only water vapor to pass to the cold side. The driving force in MD is given by the vapor pressure gradient between the hydrophobic surfaces of the membrane (Deshmukh et al. 2018; Deshmukh and Elimelech 2017a; Warsinger et al. 2017). MD processes are energy-consuming and cost-effective technologies as they have many unique features over other pressure-driven membrane separation processes such as NanoFiltration (NF) and reverse osmosis (RO) (Ghaffour et al. 2019). It also serves as a potential technique to separate organic and heavy metals contaminants from wastewater and aqueous solutions (García-Payo, Izquierdo-Gil, and Fernández-Pineda 2000; Zolotarev et al. 1994).

In this sense, an experimental test bench was built for characterization of hydrophobic membranes and evaluation of the thermal performance of flat sheet DCMD module under different operational parameters (inlet feed and permeate temperatures, inlet feed and permeate volumetric flow rates) in a fully controlled environment. The experiments were carried according to the 2k factorial experimental design, with different levels of NaCl concentration in the feed solution, where the distillate mass flux obtained experimentally were compared with the results obtained through a theoretical model for distillate flux prediction.

2. THEORETICAL MODEL

The modeling and simulation of the heat and mass transfer phenomena that occur in membrane distillation processes are crucial to theoretically evaluating the transport mechanisms and the interaction of parameters that influence the efficiency of the process. This task is essential to reduce costs and time in the experimental analysis through the variety of operational parameters, as well as to promote the optimization of the system. In this sense, in addition to the influence of membrane characteristics, one of the main factors that affects the performance of the membrane distillation process is the temperature polarization phenomenon shown in the schematic representation of Figure 1 and evaluated by the temperature polarization coefficient (CPT) obtained by:

$$CPT = \frac{T_{m,f} - T_{m,p}}{T_f - T_p} \tag{1}$$

Temperature polarization refers to the effect that the thermal boundary layer causes in reducing the temperature difference between the membrane surfaces ($T_{m,f}$ – temperature at the feed-membrane interface and $T_{m,p}$ - temperature at the membrane-permeate interface) in relation to temperature difference between the fluid streams (T_f - average temperature of the fluid in the feed stream - and T_p - average temperature of the fluid in the permeate stream). This phenomenon results in a decrease in permeate production, because of the reduction of the driving force of the process (vapor pressure gradient) and reduction of thermal efficiency.

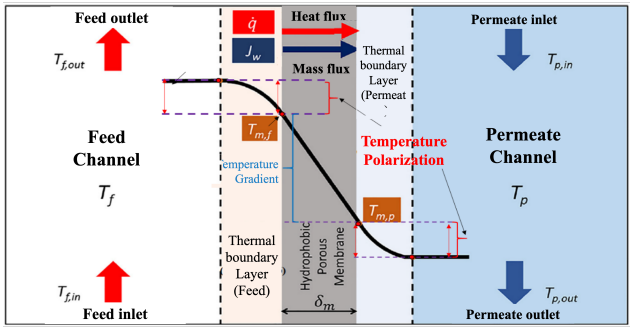

Figure 1. illustrative drawing of the temperature polarization phenomenon.
Adapted from (Yazgan-Birgi, Hassan Ali, and Arafat 2019).

2.1 Heat transfer

The heat transfer process is modeled in three regions as shown in the scheme of Figure 2: (i) the convective heat transfer ($\dot{Q}_f$) in the thermal boundary layer of the feed channel along the membrane and described by Eq. (2), (ii) the transmembrane heat transport ($\dot{Q}_m$) described by Eq. (3) and (iii) heat transfer by convection ($\dot{Q}_p$) in the thermal boundary layer of the permeate channel on the other side of the membrane.

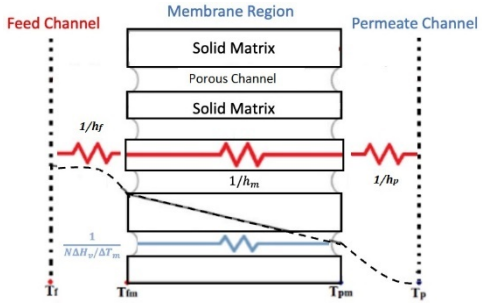

Figure 2. Schematic drawing of thermal resistances in a DCMD module. Adapted from (Srisurichan et al., 2006)

$$\dot{Q}_f = h_f A_m (T_f - T_{fm}) \tag{2}$$

$$\dot{Q_m} = A_m (N_w \Delta H_V + \frac{k_m}{\delta} (T_{fm} - T_{pm}) \tag{3}$$

$$\dot{Q}_p = h_p A_m (T_{pm} - T_p) \tag{4}$$

where $\dot{Q}$ is the heat transfer rate [W], h is the convection heat transfer coefficient [W/m² K], A_m is the area of the membrane faces [m²], N_w is the permeate flux [kg/m² s], ΔH_V is the latent heat of vaporization [J/kg], k_m is the effective thermal conductivity of the membrane [W/m K] and δ is the nominal thickness of the membrane [m]. The effective conductivity, k_m, can be estimated from the thermal conductivities of the solid and vapor phases k_{ms} and k_{mg}, and the membrane porosity ε [-] as described in the isostrain model of Eq. (5), which the literature indicates as adequate for membranes with solid and gas phases approximately parallel to each other (Ali et al. 2013; Andrjesdóttir et al. 2013; Lawson and Lloyd 1997; Marques Lisboa et al. 2021a).

$$k_m = (1 - \varepsilon) k_{ms} + \varepsilon k_{mg} \tag{5}$$

In steady-state, the three Eqs. (2), (3) and (4) can be combined to determine the surface temperatures at the membrane interfaces (T_{fm} and T_{pm}), once the heat transfer coefficients are determined, equating the heat transfer rates in each region:

$$\dot{Q}_f = \dot{Q}_m = \dot{Q}_p \tag{6}$$

By means of the energy balance of Eq. (6), and rewriting k_m/δ as h_m, the membrane surface temperatures on the feed (T_{fm}) and permeate (T_{pm}) sides can be obtained as:

$$T_{fm} = \frac{\left(h_m \left(T_p + \left(\frac{h_f}{h_p}\right) T_f\right) + h_f T_f - N_w \Delta H_V\right)}{h_m + h_f \left(1 + \frac{h_m}{h_p}\right)} \tag{7}$$

$$T_{pm} = \frac{\left(h_m \left(T_f + \left(\frac{h_p}{h_f}\right) T_p\right) + h_p T_p + N_w \Delta H_V\right)}{h_m + h_p \left(1 + \frac{h_m}{h_f}\right)} \tag{8}$$

Thus, evaluating the flow regime, laminar or turbulent, through the Reynolds number (Re), the indicated correlation was selected to calculate the Nusselt number from which it is possible to obtain the heat transfer coefficient of the channel feed and permeate as:

$$\mathrm{h} = \frac{Nu\ \mathrm{k}}{d_h} \tag{9}$$

where k is the thermal conductivity [W/m K], ρ is the density [kg/m³], μ is the dynamic viscosity [Pa.s], and c_p is the specific heat [J/kgK].

The correlations for the Nusselt number in the feed and permeate channels under laminar flow conditions, Eq. (10) (Rehm 1986), were adopted according to the models described in the literature for DCMD membrane distillation (Andrjesdóttir et al. 2013; Marques Lisboa et al. 2021b).

$$Nu = 4.36 + \frac{0{,}036RePr\left(\frac{d_h}{L}\right)}{1 + 0{,}0011\left[RePr\left(\frac{d_h}{L}\right)\right]^{2/3}} \qquad Re < 2100 \tag{10}$$

2.2 Mass transfer

The permeate flux through the membrane (N_w) can be described by the Dusty-Gas model, based on the Maxwell-Stefan relationships. Neglecting surface diffusion, the Dusty-Gas model is presented in Eq. (11), (Lawson and Lloyd 1997):

$$\frac{J_w}{D_w^k} + \frac{p_a J_w - p_w J_a}{D_{wa}^o} = -\frac{1}{RT_m}\nabla p_w \tag{11}$$

where J_w and J_a are the molar fluxes of water vapor and air [mol/m² s], p_w and p_a are the partial pressures of water vapor and air inside the pore [Pa], D_w^k is the diffusivity of Knudsen, D_{wa}^o is the molecular diffusivity of water in the air, T_m is the thermodynamic average temperature inside the pores and R is the universal gas constant.

Therefore, the permeate flow, N_w, defined by Eq. (12), is determined from the permeate molar flow, J_w, from Eq. (13), which is the result of Eq. (11) neglecting viscous transport and surface diffusion, zero airflows ($J_a \cong 0$) inside the pores and considering the Dalton's law (Deshmukh and Elimelech 2017b; Marques Lisboa et al. 2021a):

$$N_w = J_w M_w \tag{12}$$

$$J_w = C_{hidrophobicity}\frac{D_{wa}^o}{RT_m\delta}\ln\left(\frac{D_{wa}^o - D_{eff}p_a^{vap}}{D_{wa}^o - D_{eff}p_p^{vap}}\right) \tag{13}$$

where δ is the membrane thickness, M_w is the molecular mass of water D_{eff} is the effective diffusion calculated from Eq. (14), p_a^{vap} and p_p^{vap} are the partial vapor pressures at the membrane interface on the feed and permeate sides, respectively.

$$D_{eff} = \left(\frac{D_w^k D_{wa}^o}{D_{wa}^o + PD_w^k}\right) \tag{14}$$

The Knudsen diffusivity D_w^k and the molecular diffusivity of water in air D_{wa}^o are calculated from Eqs. (15) and (16), respectively:

$$D_w^k = \frac{\varepsilon d_p}{3\tau}\sqrt{\frac{8RT_m}{\pi M_w}} \tag{15}$$

$$D_{wa}^o = 4{,}46 \cdot 10^{-6}\frac{\varepsilon}{\tau}T_m^{2{,}334} \tag{16}$$

where ε is the membrane porosity, τ is the membrane tortuosity and d_p is the membrane pore diameter.

Considering that the phenomenon of capillary depression is a consequence of the hydrophobicity of the membrane, we propose the correction factor, $C_{hydrophobicity}$ [-], described by Eq. (17). The curved region formed at the entrance of the membrane pores increases the total area of the liquid-vapor interface according to the value of the contact angle, θ, which varies from membrane to membrane.

$$C_{hidrophobicity} = \frac{2}{[1 + \sin(\theta)]} \tag{17}$$

3. LABORATORY BENCH FOR MEMBRANE CHARACTERIZATION

A desalination bench was designed and built for the characterization of commercial membranes and superhydrophobic modified membranes in the membrane distillation process for the DCMD configuration.

The proposed experimental system (Figure 3) consists of two hydraulic circuits: a feed circuit described by the orange lines, where the saltwater flows, and a permeate circuit described by the blue lines, where the distilled water flows. In this configuration, the membrane is the only existing barrier that separates the feed stream from the permeate stream. The heating of the feed stream and the cooling of the permeate stream are carried out with the aid of two heat exchangers connected to two ultra-thermostatic baths to control the temperatures of both streams. The range established for the feed temperature was 65-85°C and the permeate temperature was 25-40°C. The flow rate for feed and permeate was established by the operational limit of the pumps available on the laboratory bench (0.2 – 0.8 L/min).

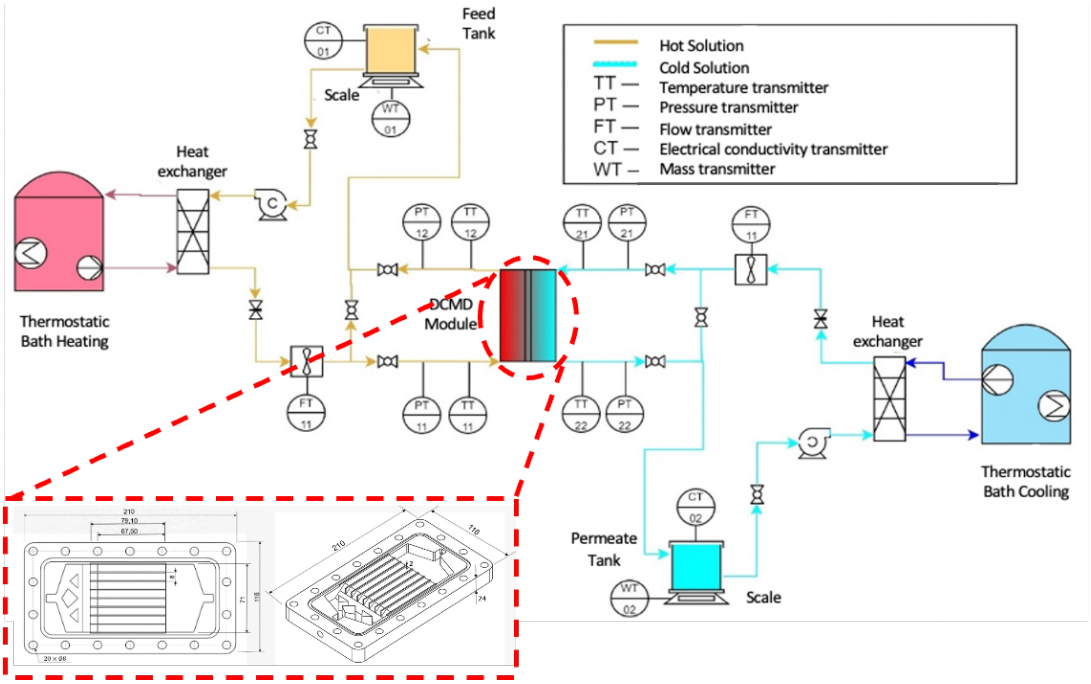

Figure 3. Schematic drawing of the benchtop membrane distillation system designed and built in the laboratory in DCMD configuration with flat sheet module.

3.1 Operating conditions in the laboratory bench and the experimental planning

Different sets of experiments were carried out to investigate the effects of fluid temperatures and feed solute concentration on the permeate flow. The parametric characterization of the experiments was carried out through the execution of the 2k factorial planning matrix with a central point, in which the operational parameters that are feed and permeate temperature and feed and permeate flow vary in the levels 65 - 85°C (feed temperature, central point 75 °C), 25 - 40°C (permeate temperature, central point 32.5 °C), and 0.2 - 0.8 L/min (feed and permeate flow, central point 0.5 L/min).

Initially, all experiments were performed with deionized water (DI) flowing in countercurrent through the two channels, feed and permeate, of the board-frame membrane module with AQUASTILL PE membrane, whose parameters are described in Table 1. All values found for the properties, presented in this table, refer to the membrane characterization process carried out.

Table 1. Properties of the membranes used in the experiment.

Parameters	Properties of the PE membrane	
	Measured	Manufacturer
Contact angle (θ)	99.5° (±2%)	NR[(1)]
Porosity (ε)	89.2% (± 4%)	85%
Porous radius (r_p)	NV [(1)]	0.16 μm[(1)]
Thickness (δ)	91 ± 10 µm	110 μm[(1)]

[(1)] Manufacturer's values (PE-AQUASTILL), NV - Not Verified, NR - Not Reported

After carrying out experiments with deionized water flowing in the feed and permeate channels with PE-AQUASTILL membranes, additional experiments were carried out under the operational conditions established for the central points in the experimental design (Table 2), using two levels of saline water concentration (initially planned as 15g/l and 35g/l of NaCl) flowing through the feed channel with the same PE-AQUASTILL membrane.

It is important to emphasize that in the permeate channel (cold side) and feed channel (hot side), the flow in both channels was characterized as in the laminar regime, with Reynolds number varying between 500<Re<2100. The hydraulic diameter (d_h) determined from the geometric characteristics of the DCMD module was 3.2 mm and the membrane specific area (A_m) is 0.005062 m².

4. RESULTS AND DISCUSSION

4.1 Verification of the experimental bench

Firstly, an important test adopted for commissioning the experimental bench is the monitoring of the mass flow rate balance, which was verified through the mass registered in the balances of the feed and permeate circuits within the determined interval of acquisition time, after reaching the steady-state regime, here considered when the variation of the parameters controlled according to the experimental design, feed and permeate inlet temperature, and feed and permeate inlet flow is less than 2% of the specified value.

Figure 4a presents the mass balance for the water that permeates through the membrane, given by relation between the water mass flow rate lost by the feed side and water mass flow rate gained by the permeate side, and Fig. 4b shows the energy balance in each side of the DCMD module, for each experiment performed. These figures shows that the experimental results obtained for the distillate mass flow are within the experimental error of ±10%, while some experimental findings for the energy balance are slightly out of this range.

The RMSE– the root mean square error – of the mass balance, for all saline concentration experimentally studied, were 0.14 g/min for the deionized water, 0.08 g/min for saltwater saline concentration of 18.6±0.8 g/L, and 0.09 g/min for saltwater saline concentration of 35.5±2.2 g/L, respectively. On the other hand, the RMSE results for the energy balance, for all experiments carried out in deionized water, 18.6±0.8 g/l and 35.5±2.2 g/l, was 0.081, 0.311 and 0.312, respectively.

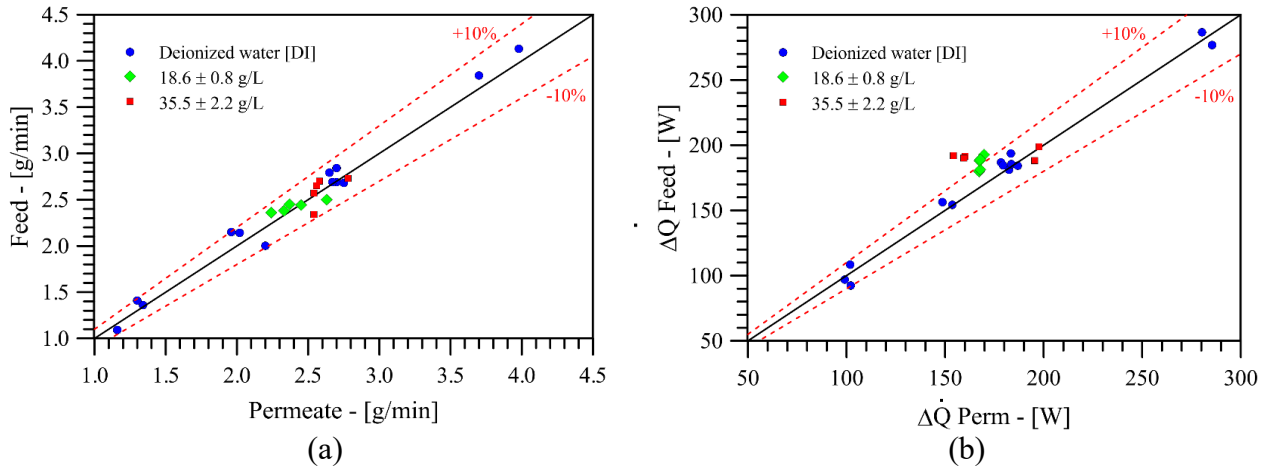

Figure 4. Checking the (a) mass balance, (b) energy balance.

4.2 Comparison of experimental results and theoretical model

The simulated experiments were obtained for five parameters: inlet temperature in the feed channel ($T_{f,in}$), inlet temperature in the permeate channel ($T_{p,in}$), feed flow at the inlet ($V_{f,in}$), permeate flow at the inlet ($V_{p,in}$) and salt concentration of the feed stream (C_{NaCl}), highlighting that the response variable is the average permeate flux (N_w), used as a parameter for comparison with the experimental results obtained on the LabMEMS laboratory bench.

The results of experiments and simulations are presented in Table 2. The model results indicate a slight decrease in permeate flow with increasing concentration, as can be seen in the simulated permeate mass flow center point values ($N_{w,simulated}$) in Table 2. This trend agrees with other studies reported in the literature on membrane distillation analysis (Andrjesdóttir et al. 2013; Lawson and Lloyd 1996; Martínez and Rodríguez-Maroto 2007).

There is a good agreement between the simulated permeate flow results ($N_{w,simulated}$) with the experimental ones ($N_{w,experimental}$) in most operational conditions evaluated, regardless of the saline concentration used. However, it is

worth noting that the model seems to underestimate the permeate flow values of the experimental results. This can be attributed to the simplification of the temperature profiles along the length of the module in the prediction of heat transfer, obtained through the correlations of the Nusselt number, used to estimate the surface temperatures in the membrane on the feed and permeate sides, but other effects may have some relevance, such as the imprecision associated with the geometric and morphological parameters of the membrane described in Table 1, which directly impact the estimation of parameters such as the effective membrane conductivity, the hydrophobicity correction coefficient or the Knudsen diffusion coefficients, D_w^k, and molecular diffusion of water in the air, D_{wa}^o, which can significantly modify the response of the DGM model in determining permeate flow.

However, it is important to note that despite apparently underestimating the flow of permeate N_w, the model values presented a mean square error of 2.52 kg/m²h in different operational settings and with concentrations of up to 35 g/L of NaCl in the feed solution, indicating a satisfactory prediction capacity for different operating conditions.

It is worth noting that to monitor the concentration of the solution in the feed tank, a calibration curve was estimated to convert the electrical conductivity measured in the feed tank to a common concentration of NaCl. The theoretical concentrations of the solutions used in the construction of the calibration curve were: 5.0 g/L; 15.0 g/L; and 35 g/L and conductivity measurements were performed using a DM-32 benchtop conductivity meter with a conductivity cell with a constant equal to 1 cm^{-1} (DIGIMED). The experimental points and the calibration curve estimated are obtained from:

$$C_{NaCl} = 0.89712\sigma - 3.7811 \quad (25)$$

where σ is the electrical conductivity [mS/cm].

Table 2. Experimental and simulated distillate mass flux for different operating parameters (2k factorial experimental).

Num. run	C_{NaCl} [g/L]	T_{in} Feed [°C]	T_{in} Permeate [°C]	$\dot{V}$ Feed [L/min]	$\dot{V}$ Permeate [L/min]	$N_{w,experimental}$ [kg/m²h]	$N_{w,simulated}$ [kg/m²h]	Relative deviation
1	0 [DI]	65.0 ± 0.8	25.0 ± 0.3	0.21 ± 0.01	0.21 ± 0.01	15.9 ± 0.3	15.80	-0.4 %
2	0 [DI]	85.0 ± 2.5	25.1 ± 0.5	0.25± 0.01	0.80± 0.01	31.1 ± 0.8	34.14	9.9 %
3	0 [DI]	65.0 ±1.3	40.0 ± 0.5	0.24± 0.01	0.82± 0.01	15.0 ± 0.3	14.01	-6.7 %
4	0 [DI]	85.3 ±1.5	39.9 ± 0.6	0.20± 0.01	0.22 ± 0.01	27.3 ± 0.8	26.46	-2.9 %
5	0 [DI]	65.0 ± 0.8	25.0 ± 0.3	0.82± 0.01	0.82± 0.01	23.3 ± 0.6	24.71	6.1 %
6	0 [DI]	85.0 ± 1.3	25.0 ± 0.4	0.81± 0.01	0.22 ± 0.01	47.5 ± 2.2	42.94	-9.6 %
7	0 [DI]	65.0 ± 0.8	40.0 ± 0.5	0.86± 0.01	0.23 ± 0.01	15.2 ± 0.3	15.49	2.2 %
8	0 [DI]	85.1 ± 1.3	40.1 ± 0.5	0.82± 0.01	0.82± 0.01	44.5 ± 2.0	43.25	-2.7 %
9 (C)	0 [DI]	75.0 ± 1.1	32.5 ± 0.4	0.54± 0.01	0.53± 0.01	32.1 ± 1.0	28.24	-12.0 %
10 (C)	0 [DI]	75.0 ± 1.9	32.6 ± 0.4	0.55± 0.01	0.54± 0.01	32.7 ± 1.1	28.52	-12.6 %
11 (C)	0 [DI]	75.1 ± 1.0	32.5 ± 0.4	0.55± 0.01	0.54± 0.01	32.2 ± 1.0	28.59	-11.1 %
12 (C)	0 [DI]	75.0 ± 1.0	32.5 ± 0.4	0.54± 0.01	0.54± 0.01	32.2 ± 1.0	28.2	-12.2 %
13 (C)	0 [DI]	74.9 ± 1.0	32.5 ± 0.4	0.53± 0.01	0.54± 0.01	31.9 ± 1.0	28.10	-11.7 %
9 (C)	18.0 ± 0.3	75.1 ± 2.0	32.5 ± 0.4	0.52± 0.01	0.52± 0.01	30.2 ± 0.8	27.95	-7.3 %
10 (C)	18.5 ± 0.3	75.0 ± 1.9	32.6 ± 0.5	0.52± 0.01	0.51± 0.01	29.1 ± 0.8	27.72	-4.6 %
11 (C)	18.5 ± 0.3	74.9 ± 1.7	32.5 ± 0.5	0.52± 0.01	0.52± 0.01	28.3 ± 0.8	27.73	-2.0 %
12 (C)	18.8 ± 0.2	75.0 ± 2.2	32.5 ± 0.5	0.52± 0.01	0.52± 0.01	28.0 ± 0.8	27.75	-0.9 %
13 (C)	19.1 ± 0.1	75.0 ± 2.0	32.5 ± 0.4	0.52± 0.01	0.52± 0.01	26.6 ± 0.7	27.77	+4.4 %
9 (C)	37.4 ± 0.2	75.1 ± 1.9	32.4 ± 0.4	0.51± 0.02	0.51± 0.01	28.1 ± 0.8	27.55	-1.9 %
10 (C)	34.9 ± 0.2	75.1 ± 1.3	32.5 ± 0.4	0.51± 0.01	0.53± 0.01	31.2 ± 0.8	27.55	-11.7 %
11 (C)	34.9 ± 0.4	75.1 ± 1.4	32.5 ± 0.4	0.51± 0.03	0.53± 0.03	30.5 ± 0.8	27.63	-9.3 %
12 (C)	35.0 ± 0.4	75.3 ± 1.6	32.6 ± 0.4	0.51± 0.03	0.53± 0.03	30.1 ± 0.8	27.74	-7.8 %
13 (C)	35.1 ± 0.3	75.1 ± 1.1	32.5 ± 0.5	0.50± 0.03	0.53± 0.03	28.3 ± 0.7	27.47	-2.7 %

For a visual comparison between the experimental and simulated results for the distillate mass flux, Fig. 5 illustrates the good agreement of this parameter, based on the 2^k factorial experiments design of Table 2.

The Pareto chart in Figure 6 shows the statistical significance of the factors evaluated and their interactions about the permeate flux. It is observed that the factors referring to the feed temperature and the feed flow showed greater significance in the response variable. Factors with values to the right on the red dashed line indicate that they should be

considered statistically significant. The factors for feed temperature and feed flow rate showed the highest significance in the response variable. However, permeate temperature and permeate flow rate can be also statistically significant. The negative value of the effect of permeate temperature in the Pareto diagram and because the response variable N_w is negatively impacted with the increase of this variable.

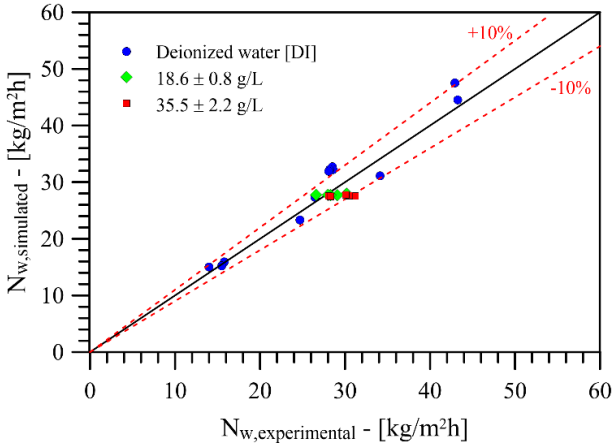

Figure 5. Comparison between the experimental and simulated distillate mass flux.

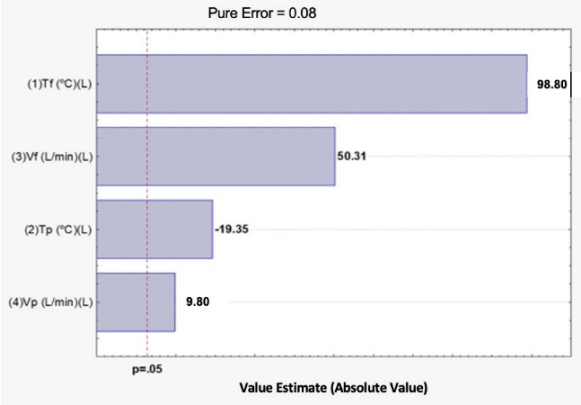

Figure 6. Pareto Chart for the standardized effects of the laboratory bench experiment.

From the analysis of the Pareto diagram, an empirical model obtained by regression allows the estimation of the studied response variable (permeate flow, N_w) for values contained in the ranges established in the experimental design. The response surfaces shown in Figure 7 were obtained from this analysis.

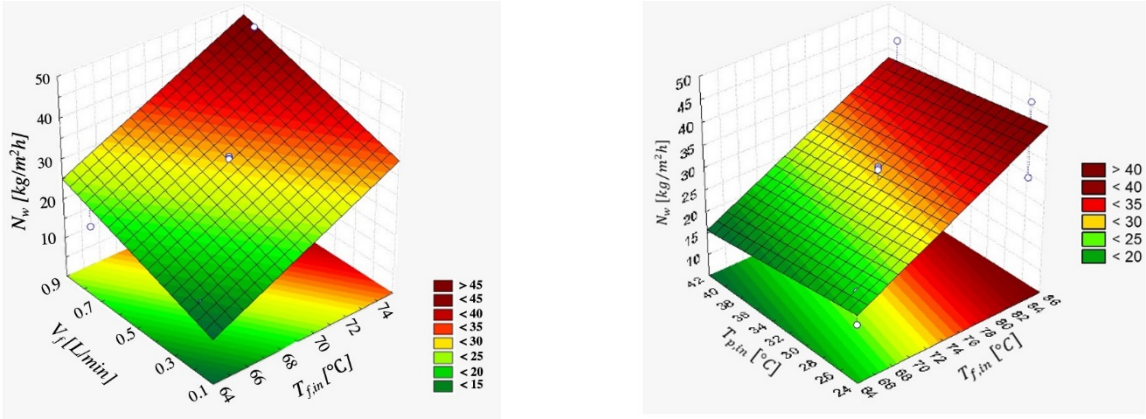

(a) (b)

Figure 7. Mean permeate flux response surface (a) N_w x (V_{feed}; T_{feed}). (b) N_w x ($T_{permeate}$; T_{feed}).

The effect of the feed temperature (T_{feed}) on the increase of the response variable as observed in Figure 7a and Figure 7b is an expected behavior, since this variable is exponentially related to the vapor pressure, markedly affecting the

pressure gradient in the thickness membrane, and thus favoring the transport of water vapor through it. The significance of the feed flow in the permeate flow was also expected, given that an increase in the net current results in a reduction in the thickness of the boundary layer, which decreases temperature polarization effects, providing greater permeate flux.

On the other hand, decreasing the permeate inlet temperatures can increase the permeate flux, however, for lower temperatures, it increases the electrical consumption of the system due to the greater need for pumping energy (higher viscosity) and eventually fluid cooling (EL -BOURAWI et al., 2006).

5. CONCLUSIONS

It can be concluded from this study of the laboratory bench of membrane distillation that the theoretical and experimental results showed good agreement with each other, in addition to having led to conclusions like those of other works with the DCMD configuration, such as a decrease in the permeate flux with increasing salinity in the feed solution.

The results also show that the inlet temperature of the feed stream and the feed flow at the inlet are the factors that exert the greatest influence on the permeate flow obtained. The first factor is directly related to the driving force of the permeate flow, due to the relationship between vapor pressure and temperature of the feed stream at the membrane interface.

Observing the values found for mass and energy balance between permeate and feed streams values, it can be concluded that they were acceptable since the results found were within the region considered satisfactory for the values, even without considering any losses to the external environment.

The comparison between the experimental results of the distillate flux and the model results indicated that there is a slight underestimation by the theoretical model, which can be attributed to the various simplifications in the model design and the inaccuracies of the input data. The main sources of these differences can be progressively evaluated through critical comparisons with the local models to be implemented via CFD for this case in the next step. Thus, it is intended to improve this lumped-parameter model (lumped model) from these observations. The lumped model is very useful for the design of desalination equipment and can be used for a first search in the optimization of the process, delimiting the search region for a simulation via CFD, enabling this tool by reducing the computational cost.

Finally, according to satisfactory experimental validation results and a good agreement between the experimental and theoretical model results, the experimental test bench developed and built in the laboratory is ready to be employed in hydrophobic membrane characterization and evaluation of the thermal performance of the flat sheet DCMD module under different operational conditions.

6. ACKNOWLEDGEMENTS

Partial funding by Petrogal Brasil Project GALP/38, and the sponsoring agencies CAPES, FAPERJ, and CAPES/PROCAD Defesa, are gratefully acknowledged.

7. REFERENCES

Ali, A., F. Macedonio, E. Drioli, S. Aljlil, and O. A. Alharbi. 2013. “Experimental and Theoretical Evaluation of Temperature Polarization Phenomenon in Direct Contact Membrane Distillation.” *Chemical Engineering Research and Design* 91(10):1966–77. DOI: 10.1016/J.CHERD.2013.06.030.

Andrjesdóttir, Ólöf, Chin Lee Ong, Majid Nabavi, Stephan Paredes, A. S. G. Khalil, Bruno Michel, and Dimos Poulikakos. 2013. “An Experimentally Optimized Model for Heat and Mass Transfer in Direct Contact Membrane Distillation.” *International Journal of Heat and Mass Transfer* 66:855–67. DOI: 10.1016/J.IJHEATMASSTRANSFER.2013.07.051.

Deshmukh, Akshay, Chanhee Boo, Vasiliki Karanikola, Shihong Lin, Anthony P. Straub, Tiezheng Tong, David M. Warsinger, and Menachem Elimelech. 2018. “Membrane Distillation at the Water-Energy Nexus: Limits, Opportunities, and Challenges.” *Energy & Environmental Science* 11(5):1177–96. DOI: 10.1039/C8EE00291F.

Deshmukh, Akshay, and Menachem Elimelech. 2017a. “Understanding the Impact of Membrane Properties and Transport Phenomena on the Energetic Performance of Membrane Distillation Desalination.” *Journal of Membrane Science* 539:458–74. DOI: 10.1016/j.memsci.2017.05.017.

Deshmukh, Akshay, and Menachem Elimelech. 2017b. “Understanding the Impact of Membrane Properties and Transport Phenomena on the Energetic Performance of Membrane Distillation Desalination.” *Journal of Membrane Science* 539:458–74. DOI: 10.1016/J.MEMSCI.2017.05.017.

El-Dessouky, Hisham T., and Hisham Mohamed. Attorney. 2002. *Fundamentals of Salt Water Desalination*. Elsevier.

Emeh, Chukwuebuka, and Ogbonnaya Igwe. 2018. “Effect of Environmental Pollution on Susceptibility of Sesquioxide-Rich Soils to Water Erosion.” *Https://Doi.Org/10.1080/24749508.2018.1452484* 2(2):115–26. DOI: 10.1080/24749508.2018.1452484.

Fan, Siyuan, Yu Wang, Shengxian Cao, Tianyi Sun, and Peng Liu. 2021. "A Novel Method for Analyzing the Effect of Dust Accumulation on Energy Efficiency Loss in Photovoltaic (PV) System." *Energy* 234:121112. DOI: 10.1016/J.ENERGY.2021.121112.

García-Payo, M. C., M. A. Izquierdo-Gil, and C. Fernández-Pineda. 2000. "Air Gap Membrane Distillation of Aqueous Alcohol Solutions." *Journal of Membrane Science* 169(1):61–80. doi: 10.1016/S0376-7388(99)00326-9.

Ghaffour, N., S. Soukane, J. G. Lee, Y. Kim, and A. Alpatova. 2019. "Membrane Distillation Hybrids for Water Production and Energy Efficiency Enhancement: A Critical Review." *Applied Energy* 254.

Huo, Jinrong, Ling Fu, Chenxu Zhao, and Chaozheng He. 2021. "Hydrogen Generation of Ammonia Borane Hydrolysis Catalyzed by Fe22@Co58 Core-Shell Structure." *Chinese Chemical Letters* 32(7):2269–73. doiDOI: 10.1016/J.CCLET.2020.12.059.

Hwang, Ho Jung, Ke He, Stephen Gray, Jianhua Zhang, and Il Shik Moon. 2011. "Direct Contact Membrane Distillation (DCMD): Experimental Study on the Commercial PTFE Membrane and Modeling." *Journal of Membrane Science* 371(1–2):90–98. DOI: 10.1016/J.MEMSCI.2011.01.020.

Khayet, M., M. P. Godino, and J. I. Mengual. 2002. "Thermal Boundary Layers in Sweeping Gas Membrane Distillation Processes." *AIChE Journal* 48(7):1488–97. doiDOI: 10.1002/AIC.690480713.

Lawson, Kevin W., and Douglas R. Lloyd. 1996. "Membrane Distillation. II. Direct Contact MD." *Journal of Membrane Science* 120(1):123–33. DOI: 10.1016/0376-7388(96)00141-X.

Lawson, Kevin W., and Douglas R. Lloyd. 1997. "Membrane Distillation." *Journal of Membrane Science* 124(1):1–25. DOI: 10.1016/S0376-7388(96)00236-0.

Li, Xiaowei, Chenlu Zhang, Beibei Zhang, Di Wu, Dandan Zhu, Wei Zhang, Qing Ye, Junhua Yan, Juemin Fu, Chengliang Fang, Denglong Ha, and Shenglei Fu. 2021. "Nitrogen Deposition and Increased Precipitation Interact to Affect Fine Root Production and Biomass in a Temperate Forest: Implications for Carbon Cycling." *Science of The Total Environment* 765:144497. DOI: 10.1016/J.SCITOTENV.2020.144497.

Li, Zhiguo, Jie Wang, and Shuai Che. 2021. "Synergistic Effect of Carbon Trading Scheme on Carbon Dioxide and Atmospheric Pollutants." *Sustainability 2021, Vol. 13, Page 5403* 13(10):5403. DOI: 10.3390/SU13105403.

Marques Lisboa, Kleber, Diego Busson de Moraes, Carolina Palma Naveira-Cotta, and Renato Machado Cotta. 2021a. "Analysis of the Membrane Effects on the Energy Efficiency of Water Desalination in a Direct Contact Membrane Distillation (DCMD) System with Heat Recovery." *Applied Thermal Engineering* 182:116063. DOI: 10.1016/J.APPLTHERMALENG.2020.116063.

Marques Lisboa, Kleber, Diego Busson de Moraes, Carolina Palma Naveira-Cotta, and Renato Machado Cotta. 2021b. "Analysis of the Membrane Effects on the Energy Efficiency of Water Desalination in a Direct Contact Membrane Distillation (DCMD) System with Heat Recovery." *Applied Thermal Engineering* 182:116063. DOI: 10.1016/J.APPLTHERMALENG.2020.116063.

Martínez, L., and J. M. Rodríguez-Maroto. 2007. "Effects of Membrane and Module Design Improvements on Flux in Direct Contact Membrane Distillation." *Desalination* 205(1–3):97–103. doi: 10.1016/J.DESAL.2006.02.050.

Moondra, N., Namrata D. J., and Robin A. C. 2021. "Role of Phytoremediation in Domestic Wastewater Treatment." *Water Conservation and Management* 35–39.

Phattaranawik, J., R. Jiraratananon, and A. G. Fane. 2003. "Heat Transport and Membrane Distillation Coefficients in Direct Contact Membrane Distillation." *Journal of Membrane Science* 212(1–2):177–93. DOI: 10.1016/S0376-7388(02)00498-2.

Rehm, Thomas R. 1986. "High-Pressure Measurement Techniques." *Nuclear Technology* 73(1):130–130. DOI: 10.13182/NT86-A16214.

Warsinger, David M., Amelia Servi, Grace B. Connors, Musthafa O. Mavukkandy, Hassan A. Arafat, Karen K. Gleason, and John H. Lienhard. 2017. "Reversing Membrane Wetting in Membrane Distillation: Comparing Dryout to Backwashing with Pressurized Air." *Environmental Science: Water Research & Technology* 3(5):930–39. doi: 10.1039/C7EW00085E.

Wu, Yih Chyng, Jianglin Ye, Gengping Jiang, Kun Ni, Na Shu, Pierre Louis Taberna, Yanwu Zhu, and Patrice Simon. 2021. "Electrochemical Characterization of Single-Layer Graphene/Electrolyte Interface: Effect of Solvent on the Interfacial Capacitance." *Angewandte Chemie International Edition* 60(24):13317–22. DOIDOI: 10.1002/ANIE.202017057.

Yazgan-Birgi, Pelin, Mohamed I. Hassan Ali, and Hassan A. Arafat. 2019. "Comparative Performance Assessment of Flat Sheet and Hollow Fiber DCMD Processes Using CFD Modeling." *Separation and Purification Technology* 212:709–22. DOI: 10.1016/J.SEPPUR.2018.11.085.

Zolotarev, P. P., V. v. Ugrozov, I. B. Volkina, and V. M. Nikulin. 1994. "Treatment of Waste Water for Removing Heavy Metals by Membrane Distillation." *Journal of Hazardous Materials* 37(1):77–82. DOI: 10.1016/0304-3894(94)85035-6.

8. RESPONSIBILITY NOTICE

The authors are the only ones responsible for the printed material included in this paper.